AALBORG UNIVERSITY

Electronic Energy Transfer in Polarizable Heterogeneous Environments: A Systematic Investigation of Different Quantum Chemical Approaches

Steinmann, Casper; Kongsted, Jacob

Electronic Energy Transfer in Polarizable Heterogeneous Environments: A Systematic Investigation of Different Quantum Chemical Approaches

Casper Steinmann[*] and Jacob Kongsted

University of Southern Denmark, Department of Physics, Chemistry and Pharmacy, DK-5230 Odense M, Denmark

E-mail: css@sdu.dk

Abstract

Theoretical prediction of transport and optical properties of protein-pigment complexes is of significant importance when aiming at understanding the structure versus function relationship in such systems. Electronic energy transfer (EET) couplings represent a key property in this respect since such couplings provide important insight into the strength of interaction between photo-active pigments in protein-pigment complexes. Recently, attention has been payed to how the environment modifies or even controls the electronic couplings. To enable such theoretical predictions, a fully polarizable embedding model has been suggested (C. Curutchet, A. Muñoz-Losa, S. Monti, J. Kongsted, G. D. Scholes, and B. Mennucci, J. Chem. Theory Comput., 2009 5 (7), 1838-1848). In this work, we further develop this computational model by extending it with an ab initio derived polarizable force field including higher-order multipole moments. We use this extended model to systematically examine three different ways of

1

obtaining EET couplings in a heterogeneous medium ranging from use of the exact transition density to a point-dipole approximation. Several interesting observations are made including that explicit use of transition densities in the calculation of the electronic couplings - also when including the explicit environment contribution - can be replaced by a much simpler transition point charge description without comprising the quality of the model predictions.

1 Introduction

Electronic energy transfer (EET) is the process by which an excitation of a pigment is transferred to another pigment. EET plays an important role in the light-harvesting process of photosynthesis, where a multitude of photoactive antennae harvest sunlight and funnel it to a reaction center to initiate an overall charge separation process.[1,2] In order to enable theoretical predictions of energy transfer pathways and optical spectra of protein-pigment complexes (PPCs), one computational strategy is to construct the Frenkel exciton Hamiltonian for a set of interacting pigments.[3] In this exciton model, the Hamiltonian includes two quantities: site energies and electronic couplings between the excited states of the pigments in the PPCs. In addition, more advanced models also take into account the explicit vibrational states of the protein and the pigments and how they couple to the excited states of the pigments (see for example references 4 and 5). Various strategies for obtaining accurate site energies have been attempted by taking the protein environment into account ranging from focused methods such as cluster models[6], where part of the protein structure is explicitly included in the quantum mechanical calculation, over point-charge embedding schemes to polarizable continuum methods.[7–13] More elaborate all quantum mechanical approaches have also recently been applied such as frozen density embedding.[14] The importance of accurate site energies have been studied extensively and each of the above approaches have their own merits.[15] In this work, we will use a focused approach with the recently developed polarizable embedding (PE) method[16,17] which takes into account the explicit environmental

response, based on a linear response scheme, upon excitation through a classical polarizable embedding potential.

The EET couplings, as first suggested by Förster[18], describe the transfer of excitation energy from one pigment to another in close proximity. The evaluation of the EET Coulomb couplings can be done in different ways using approximations such as the point-dipole approximation (PDA)[18], also termed ideal dipole approximation, which is based directly on the work by Förster and uses transition dipole moments to evaluate the Coulomb couplings.[19] The PDA model, however, breaks down when the inter-chromophoric distances become less than the dimension of the chromophores.[20] A more elaborate method is the transition density cube method which provides a way of evaluating the Coulomb couplings using charge-distributions evaluated on a large number of points around each pigment.[21] The computational demand of the transition density cube method, however, has led to the development of attractive alternative approaches to evaluate the couplings through a Coulomb expression involving only partial charges (technically transition monopoles) fitted to reproduce the electrostatic potential of the transition densities (TrESP)[22] and later extended to include higher order multipole moments.[23] Finally, the couplings can be evaluated using the transition densities directly in a Coulomb expression.[24,25]

So far, the electronic couplings have here only been discussed in terms of vacuum calculations, i.e. a direct coupling without considering the environment in which the EET takes place. To obtain reliable theoretical predictions in the condensed phase several approaches have been attempted including determining an empirical scaling factor, rescaling the transition dipole (or monopole) moments, or estimation of such scaling factors based on treating the protein environment as a dielectric continuum characterized by a dielectric constant ($\varepsilon = 2$).[10,11,26] Recently, a linear response (LR) approach within a density functional theory framework was presented where the Coulomb exciton couplings are corrected by treating the environment as a perturbation to the vacuum couplings. This model was first introduced within a very simplified continuum description of the solvent.[24] Later, this LR approach was

formulated with the polarizable continuum model (PCM) for homogeneous solvents, which allowed for a consistent treatment of solvent effects on both the excited states (site energies) and the computed EET couplings.[27–29] However, in heterogeneous systems such as light-sensitive proteins, which is the focus of this work, the PCM is less adequate and an explicit atomistic representation of the protein is preferred. Along the same lines as the PCM-LR approach, a linear response formulation in a combined quantum mechanics and molecular mechanics (QM/MM) framework was presented[13,30]. Here, the pigment of interest is treated at a quantum mechanical level of theory and the protein (and other pigments) are described by a classical polarizable force field.

This latter QM/MM approach is particularly interesting because it allows for a flexible treatment of both the QM region and the heterogeneous environment. When EET couplings are calculated using a QM/MM approach the embedding is usually based on a simple point charge scheme taken from traditional all atom force fields and an isotropic dipole-dipole polarizability is included to describe the polarization of the protein in response to the QM region.[25] In this work, the polarizable embedding method, formulated within the framework of density functional theory (PE-DFT), is used to evaluate the EET couplings. The environment is here treated using an ab initio derived force field. Contrary to the previous approach[13,30], the electrostatic part is described using an atom centered distributed multipole expansion up to and including quadrupoles. At the same expansion points, distributed anisotropic electric dipole-dipole polarizabilities are placed which gives rise to induced dipole moments. We have recently shown that the quality of the embedding potential has a profound impact on obtaining, e.g. converged NMR shielding constants[31]. In light of this, we here show the importance of utilizing an accurate embedding potential that is derived from first principles and which can reproduce the true quantum mechanical embedding potential and is not taken from a traditional protein force field.[32] Such a potential also accurately models the structural fluctuations in the embedding parameters. We note that the PE model is formulated such that the environment is allowed to relax upon electronic excitation/de-

excitation of the QM region. For completeness we mention the recent work by König and Neugebauer who presented spectra of the Fenna-Matthews-Olson (FMO) protein based on the frozen density embedding approach[14,33–35] but refer to several recent reviews for more detailed discussions on both site-energies and couplings for the exciton Hamiltonian.[5,36,37]

In this paper we will use the FMO protein complex as a test system aiming to perform a systematic investigation of different quantum chemical approaches for the calculation of the electronic couplings as well as show the importance of using an accurate embedding potential. The FMO protein complex was the first PPC to have its structure determined using X-ray spectroscopy[38,39] and has as such been the focus of many investigations regarding EETs. Structurally, the FMO complex consists of three identical protein sub-units arranged in C_3 symmetry, each binding seven Bachteriochlorophyll-a (BChla) pigments internally in the structure with an eighth pigment located between the different protein sub-units.[40,41] In this work, we only consider the seven pigments arranged inside a single protein unit (see Figure 1).
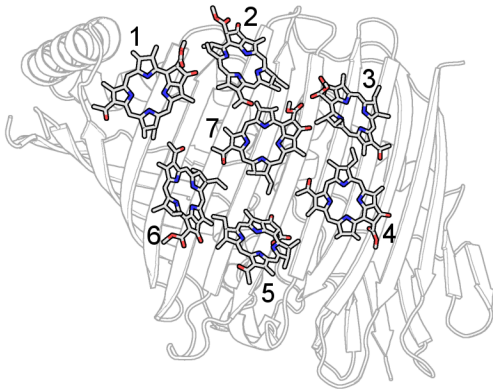
Figure 1: Schematic representation of the Fenna-Matthews-Olson protein complex used in this study here shown with the 7 included pigments numbered 1 through 7.

This paper is organized as follows. In Section 2 we outline the theoretical background to evaluate the electronic energy transfer couplings in a heterogeneous environment at different levels of theory. This is followed, in Section 3, by a brief discussion of the computational methodologies involved. We then proceed to discuss our findings in Section 4 with emphasis

on the quality of the obtained EET couplings and how the EET couplings influence a simulated absorption spectrum. Finally, in Section 5 we summarize our findings and give an outlook on possible future directions.

2 Theory

The collective excitation across multiple pigments in a photoactive system is beautifully described in the framework of excitons as first suggested by Frenkel in the 1930'ies.[3] Here, the excited state of M pigments is described through Hartree products of the m'th pigment in the p'th excited state, ϕ_m^p, and the remaining $M-1$ pigments in their ground states, i.e.

$$\Phi_m^p = \phi_m^p \prod_{n \neq m} \phi_n^0 = \phi_1^0 \phi_2^0 \ldots \phi_m^p \ldots \phi_M^0. \tag{1}$$

The k'th exciton is a linear combination of all possible excited state product wave functions

$$\Psi^k = \sum_{m=1}^{M} \sum_p C_{m,p}^k \Phi_m^p, \tag{2}$$

where the sum over p is excitations. The excited states, ϕ_m^p, are assumed to be known and the task is to find the coefficients $C_{m,p}^k$ by diagonalizing the Hamiltonian matrix of the system. In this work, we will only consider the single-exciton manifold, i.e. only one pigment is excited at any one time, in which case the exciton Hamiltonian takes the form

$$\hat{H} = \sum_{m=1}^{M} \sum_p \epsilon_{m,p} \hat{a}_{m,p}^\dagger \hat{a}_{m,p} + \sum_{m=1}^{M} \sum_{n \neq m}^{M} \sum_{p,q} J_{mn}^{pq} \left(\hat{a}_{m,p}^\dagger \hat{a}_{n,q} + \hat{a}_{n,q}^\dagger \hat{a}_{m,p} \right), \tag{3}$$

where $\epsilon_{m,p}$ is the *site-energy* of the p'th excited state of pigment m, $\hat{a}_{m,p}^\dagger$ and $\hat{a}_{m,p}$ are second quantization bosonic creation and annihilation operators, respectively which transfers an excited p state between pigments m and n. The site energy for pigment m will in most models have an expression like[42,43] $\epsilon_{m,p} = \Delta E_{m,p}^{\mathrm{vac}} + J_m + \delta_m$, where $\Delta E_{m,p}^{\mathrm{vac}}$ is the vacuum

excitation energy, J_m is a displacement term and corrects the excitation energies because of the environment in which the excitation takes place and δ_m is a fluctuation term that takes into account the variation in excitation energies due to geometrical distortions of the pigment. Instead of including the fluctuation term explicitly, the same effect can obtained by running a molecular dynamics (MD) simulation and, based on structures extracted from such an MD run, perform the requiblack calculations of the site energies. In this work we use a linear response formalism in a polarizable embedded TDDFT framework, i.e. PE-TDDFT, such that the displacement term is automatically included in the calculated excitation energies to give the following site energies

$$\epsilon_{m,p} = \Delta E_{m,p},\tag{4}$$

and we will therefore not consider the fluctuation term. The term J_{mn}^{pq} in eq 3 is the coupling of the excited states p and q on pigments m and n, respectively. As already stated, the pigments are embedded in an explicit polarizable environment that represents the protein. The EET couplings, when embedded in a polarizable environment, is written as[24,30]

$$J_{mn} = J_{mn}^{(0)} + J_{mn}^{(1)},\tag{5}$$

where we have removed the explicit reference to the excited states p and q for a simpler notation. The zero'th order term in eq 5 governs the direct interaction between the pigments and is given as

$$J_{mn}^{(0)} = \iint \mathrm{d}\mathbf{r}_1\mathrm{d}\mathbf{r}_2\,\rho_m^T(\mathbf{r}_1)\left(\frac{1}{|\mathbf{r}_1 - \mathbf{r}_2|} + g_{XC}(\mathbf{r}_1,\mathbf{r}_2)\right)\rho_n^T(\mathbf{r}_2) - \omega_0\int \mathrm{d}\mathbf{r}_1\,\rho_m^T(\mathbf{r}_1)\rho_n^T(\mathbf{r}_1).\tag{6}$$

Here the first term of the above equation constitutes the Coulomb and exchange-correlation interaction of the coupling and involves integrating over transition densities ρ_m^T and ρ_n^T of pigments m and n, respectively. The last term is the overlap and ω_0 is the transition energy.

The first order term, which is the interaction mediated by the polarizable environment, is[30]

$$J_{mn}^{(1)} = -\sum_{k}^{n_{pol}} \left(\int d\mathbf{r}_1 \, \rho_m^T(\mathbf{r}_1) \frac{\mathbf{r}_k - \mathbf{r}_1}{|\mathbf{r}_k - \mathbf{r}_1|^3} \right) \boldsymbol{\mu}_k^{ind}(\rho_n^T). \tag{7}$$

Here, the electric field caused by the transition density of pigment m interacts with n_{pol} induced dipoles at polarizable sites k in the environment due to the transition density of pigment n. Formally, the induced dipoles are determined from a set of coupled linear equations which in matrix form can be expressed as

$$\boldsymbol{\mu}^{ind}(\rho_n^T) = \mathbf{A}\mathbf{F}\left(\rho_n^T\right) \tag{8}$$

where $\mathbf{A}$ is the classical response matrix and $\mathbf{F}$ is the electric field (transition field), at the polarizable sites, from the electronic transition density of pigment n, ρ_n^T. Both $\boldsymbol{\mu}^{ind}$ and $\mathbf{F}$ are super vectors of size $3 \cdot n_{pol}$. Likewise, the integral over the transition density of pigment m (eq 7) is the transition electric field at polarizable sites k. Using the same super vector notation, the first order coupling term $J_{mn}^{(1)}$ becomes

$$J_{mn}^{(1)} = -\mathbf{F}\left(\rho_m^T\right) \mathbf{A}\mathbf{F}\left(\rho_n^T\right). \tag{9}$$

If the pigments are well separated, the approximation to include only the Coulomb coupling in the zero-order term (eq 6) is can be invoked

$$J_{mn}^{(0)} \approx \iint d\mathbf{r}_1 d\mathbf{r}_2 \, \rho_m^T(\mathbf{r}_1) \left(\frac{1}{|\mathbf{r}_1 - \mathbf{r}_2|} \right) \rho_n^T(\mathbf{r}_2). \tag{10}$$

We note that applying this Coulomb-approximation to $J_{mn}^{(0)}$ leaves the embedding term, $J_{mn}^{(1)}$, unchanged. In the remaining part of this paper we will use eq 10 as a reference when calculating $J_{mn}^{(0)}$.

When the Coulomb-approximation (eq 10) holds, a popular and less expensive method to

evaluate the couplings is to represent the transition densities of each pigment $\left(\rho_n^T\right)$ as a set of atomic partial charges $\{q_n^T\}$. In principle, any set of partial charges which reproduces the transition density potential can be used and here we use charges that are fitted to reproduce the electrostatic potential of the transition density. The approach is discussed in detail in the Appendix and is similar to that of TrESP first pioneeblack by Madjet and Renger.[22] The coupling, in terms of sets of atomic partial charges $\{q_m^T\}$ and $\{q_n^T\}$ for pigments m and n, respectively, is thus given as

$$J_{mn}^{(0)} \approx \sum_{i \in m} \sum_{j \in n} \frac{q_i^T q_j^T}{|\mathbf{R}_i - \mathbf{R}_j|}. \tag{11}$$

Describing the transition densities with the fitted charges also changes the first order couplings (eq 7) to

$$J_{mn}^{(1)} \approx -\mathbf{F}\left(\{q_m^T\}\right) \mathbf{A} \mathbf{F}\left(\{q_n^T\}\right). \tag{12}$$

That is, the transition electric field, $\mathbf{F}$, at the n_{pol} polarizable points are evaluated from the transition density charges located on the atoms of each pigment.

A final expression for the calculation of the couplings is through the point-dipole approximation by using the transition dipoles directly. Here, the transition dipoles are assumed to be located at the center of mass, $\mathbf{R}^{cm}$, of each pigment which gives the following expression for the coupling

$$J_{mn}^{(0)} \approx \boldsymbol{\mu}_m^T T_{mn}^{(2)} \boldsymbol{\mu}_n^T. \tag{13}$$

Here, the interaction tensor $T_{mn}^{(2)}$ is defined as

$$T_{mn}^{(2)} = \nabla_m^2 \frac{1}{|\mathbf{R}_m^{cm} - \mathbf{R}_n^{cm}|}. \tag{14}$$

In this scheme, the expression for the first order coupling is changed accordingly

$$J_{mn}^{(1)} \approx -\mathbf{F}\left(\boldsymbol{\mu}_m^T\right) \mathbf{A} \mathbf{F}\left(\boldsymbol{\mu}_n^T\right). \tag{15}$$

Here, the transition electric field, $\mathbf{F}$, at the polarizable sites are evaluated from the transition dipole moments located at the center of mass for each pigment. In the following we will use the three strategies presented above for computing the electronic couplings and inspect their performances.

2.1 Exciton Properties

Having obtained both the site energies and EET couplings, the exciton Hamiltonian (eq 3) is constructed and diagonalized to find the collective eigenvectors and eigenvalues (excitonic transition energies) from which the k'th exciton wavefunction (eq 2) is readily constructed. Similarly, the excitonic electric transition dipole moment, $\boldsymbol{\mu}_k^T$, for the k'th exciton is given as

$$\boldsymbol{\mu}_k^T = \sum_{m=1}^{M} \sum_p C_{m,p}^k \boldsymbol{\mu}_{m,p}^T, \tag{16}$$

from which it is possible to construct the linear absorption stick spectrum from the oscillator strengths of the k'th excited state

$$f_k = \frac{2}{3} \Delta E_{m,p}^k \left| \boldsymbol{\mu}_k^T \right|^2. \tag{17}$$

3 Computational details

3.1 Computational Strategy

To evaluate the EET couplings in the exciton Hamiltonian for the FMO protein, we used the following computational strategy: (i) From the molecular structure of the FMO protein a classical potential, represented by distributed multipole moments and polarizabilities, is evaluated for all pigments and the protein (see embedding potential details below). (ii) A single pigment is then chosen to be treated by PE-TDDFT. The classical potentials of the other pigments and the protein are combined to generate the corresponding embedding po-

tential. (iii) From the embedded excited state PE-TDDFT calculation, extract one or more of the following properties: site energies, transition densities, transition moments, transition density fitted charges and (transition) electric fields at the polarizable sites from the transition density. Steps (ii) and (iii) are repeated each pigment. (iv) Evaluate the direct couplings, $J_{mn}^{(0)}$, by either the transition densities directly (eq 10), the transition density fitted charges (eq 11) or the transition dipole moments (eq 13). (v) Evaluate the screening of the couplings, $J_{mn}^{(1)}$, by either the transition densities directly (eq 9), the transition density fitted charges (eq 12) or the transition moments (eq 15). (vi) Finally, construct the exciton Hamiltonian matrix using the quantities calculated above, diagonalize it to obtain the coupling coefficients and evaluate coupled properties of interest; e.g. the coupled transition moments or spectra.

3.2 Embedding Potential

The structure of the FMO protein from *Prosthecochloris aestuarii* (PDB: 3EOJ[40], here, a geometry optimized structure from previous work by List et al. is used[44]) consists of two chains (A and B) and was alteblack in the following ways with the Maestro[45] suite in preparation for the QM derived force field described below: An N209G mutation was introduced in the B chain in order to remove a steric clash reported by the software. The clash was most likely an artifact from the optimization procedure from the previous work. The termini on both the A and the B chains were rebuilt into their charged states. The overall charge of the system is unchanged by these modifications.

The embedding potential for the protein (the potentials for the pigments are discussed below) is generated using a fragmentation procedure, explained in detail below, that is similar to that of Söderhjelm and Ryde[46] which in turn builds on ideas from the molecular fractionation with conjugate caps[47] (MFCC) to build the potential. The protein is fragmented between the amide and the carboxyl carbon such that each residue is assigned a fragment. Each fragment that is covalently bound to a neighboring fragment is appropriately capped

with capping groups built from the neighboring fragments in accordance with the MFCC principle. This satisfies the valency of the broken bonds between fragments. In this work, we have exclusively used capping groups of N-methyl and acetyl. In addition to the capped fragments, the caps are also joined to form conjugate cap fragments. An illustration of the capping procedure can be seen in Figure 2. Atoms marked with Hc are heavier atoms converted to hydrogen atoms where the bond are scaled to an appropriate distance based on the bond type, i.e. 1.09 Å for CH bonds, 1.01 Å for NH bonds and 1.35 Å for SH bonds. Although the MFCC method was originally envisioned to be used for interaction energies, Söderhjelm and Ryde applied this method to derive potentials constructed from overlapping fragments in the following way. A property P on atom A, P^A, is calculated as[46]

$$P^A = \sum_{f=1}^{N_f} P_f^A - \sum_{f=c}^{N_c} P_c^A.$$ (18)

Here, P_f^A is the property of interest on atom A in the fth fragment and P_c^A is the property of interest on the cth conjugate cap fragments. N_f and N_c are the number of fragments and conjugate cap fragments that contain atom A, respectively. Terminating hydrogens (Hc atoms in Figure 2) are consideblack equivalent to the atoms that they replace in terms of properties when using eq 18. The embedding potential, i.e. the protein and the inactive
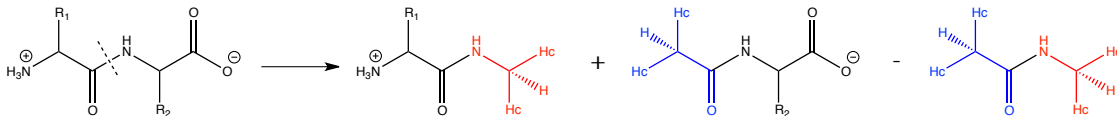

Figure 2: The molecular fractionation with conjugate caps (MFCC) here shown for the cutting (far left), capping (middle) and conjugate cap (far right) of a peptide bond. Figure taken from reference 48.

pigments are described using distributed multipole moments up to and including quadrupoles as well as distributed anisotropic electric-dipole polarizabilities located at the atomic centers. The classical parameters were evaluated at the B3LYP[49–51]/6-31+G*[52–54] level of theory using the LoProp[55] procedure in MOLCAS[56,57].

In a similar way, the pigments were also subjected to fragmentation in the phytyl chain. This was done in order to increase computational efficiency when deriving the classical parameters. Each pigment was fragmented at atoms C1, C6 and C54, C55 using FragIt[58] (see Figure S1 in the supporting information) and subject to the same methodology as for the protein above to obtain the classical parameters.

3.3   Electronic Structure Calculations

In order to increase computational efficiency, only the chromophore part of the BChl pigments were included in the quantum mechanical calculations and the phytyl chain is always treated classically (see the section above). The BChl were cut at the C1 atom and capped appropriately with a hydrogen atom. In order to avoid a polarization catastrophe, any atom in the MM region within 2.3 Å of the pigment treated by QM had its atomic properties blackistributed in such a way that static dipoles, quadrupoles and dipole polarizabilities were removed and any partial charge was divided equally among the three closest neighbors outside the 2.3 Å border.

For all excited state calculations we used a linear response time-dependent density functional theory (TDDFT) description.[16,17] Based on the work by List and co-workers[44] we employed the PBE0[59] and CAM-B3LYP[60] density functionals for the evaluation of the excited state energies, transition densities and transition dipole moments. The site energies are obtained through TDDFT as the energy of the excited state. Thus, we include electrostatic (and polarization) contributions from the environment to the site energies. These calculations were performed using DALTON.[61,62] The evaluation of the exact Coulomb coupling (eq 10) has been implemented in DALTON through the polarizable embedding library (PElib).[63] Transition density fitted charges were also evaluated in DALTON through the QFITLIB module[64] and fitted charges were constrained to sum to zero and to reproduce the transition dipole moment upon excitation. We used the 6-31+G* basis set in all calculations.

4 Results and discussion

The main focus of this work is on the evaluation of the EET couplings between pigments in the FMO protein using various strategies as presented in the theory section. The analysis of the EET couplings will begin from Section 4.2. However, Section 4.1 is devoted to the evaluation of the site energies and transition dipole moments of the individual pigments upon embedding in the protein based upon earlier work by List et al.[44] We finish by presenting a computed absorption spectrum in Section 4.3.

4.1 Site energies

Compared to the previous study by List et al., which used an OPLS-2005 point charge embedding scheme[65], we here use an embedding potential derived by quantum mechanical calculations. This embedding potential is represented by a distributed multipole expansion up to and including quadrupoles placed on each nuclei of the protein and electric dipole-dipole polarizabilities, also located on atoms. Figure 3 shows computed Q_y excitation energies of
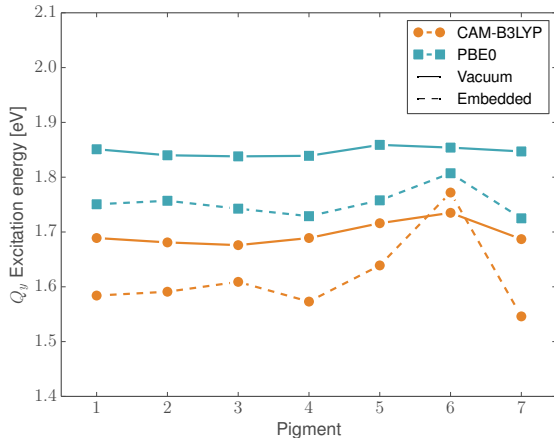

Figure 3: Computed Q_y excitation energies of the seven BChl pigments in vacuum (solid lines) and embedded in the fully polarizable protein (dashed lines).

the seven BChl pigments in the FMO protein obtained both in vacuum and embedded in the protein. We observe, in general, a red-shift of approximately 0.10 eV (see Table S2 in the

supporting information) in the excitation energy of all pigments except pigment 6 which is only red-shifted 0.06 eV and blue-shifted 0.04 eV for PBE0 and CAM-B3LYP, respectively. The blue-shift of pigment 6 has been observed before and it is speculated that the positively charged R95 acts as a hydrogen bond donor which destabilizes the excited state of this pigment.[66] However, in a recent study by Jurinovich et al.[25] the blue-shift for pigment 6 is not observed, but instead the excitation energies of all the pigments are red-shifted by 0.10 eV. Their results are based on a molecular dynamics simulation which suggests that the optimized structure, at least around pigment 6, is not representative of a situation where the protein is flexible and might be due to optimizing only the pigments using quantum mechanics while the protein is given as a simple point charge description. Interestingly, the blue-shift is here only observed for the CAM-B3LYP functional whereas it was previously also reported for the PBE0 functional on the same optimized structure.[44] By including only the static part of the embedding potential, represented by a distributed multipole expansion up to and including quadrupoles, we observe that both PBE0 and CAM-B3LYP predict a blueshift for pigment 6 of 0.001 eV and 0.09 eV, respectively, and the excitation energies are shifted significantly less than when polarization is included. Interestingly, for pigment 6, by keeping the ground state polarization frozen upon excitation, CAM-B3LYP yields a blue-shift of 0.11 eV which suggests that the polarization response of the environment upon excitation is the most important factor for the stabilization of the excited state. A similar observation is made for PBE0. Figure 4 shows transition dipole moments of the Q_y electronic excitation. As was observed for the excitation energies, a noticeable change in the transition dipole moments is observed when including the protein environment. In general, the magnitude of the transition dipole moments are increased by 1.4 Debye for both the PBE0 and CAM-B3LYP density functionals. This is in contrast to the static embedded case where the average change is well below 0.1 Debye (see Table S3 in the supporting information). Focusing on pigment 6 again, the change in magnitude of the transition dipole moment is 1.2 Debye for PBE0 (1.0 Debye for CAM-B3LYP) which again suggests that this specific
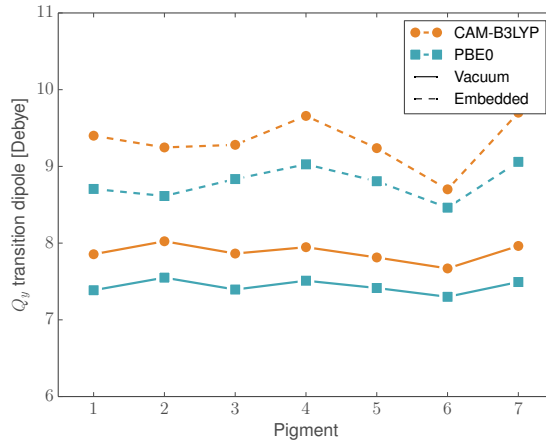
Figure 4: Computed Q_y transition dipole moments of the seven BChl pigments in vacuum (solid lines) and embedded in the fully polarizable protein (dashed lines).

pigment is perhaps not in a representative environment. Finally we note, that even though the magnitude of the transition dipoles are much larger with polarization than without, the PBE0 functional shows less variation in the obtained transition dipole moments compared to CAM-B3LYP, in agreement with previous work[44]. Based on the above analysis, the computed EET couplings will only be discussed at the PE-PBE0/6-31+G* level of theory. Couplings based on other levels of theory are presented in the supporting information.

4.2 Couplings

We now continue to present computed electronic couplings. We will initially be focused on the direct couplings, $J_{mn}^{(0)}$, followed by the screening $J_{mn}^{(1)}$. Finally we discuss the total couplings and contrast our results to other recent studies.

In Figure 5, unsigned electronic couplings, $J_{mn}^{(0)}$, calculated using the exact Coulomb expression (eq 10) are presented and correlated with the two approximate methods for evaluating the electronic energy transfer couplings: The transition dipole moment expression (eq 13) and the expression with transition density fitted charges (eq 11). We observe from Figure 5 that the couplings obtained with the transition density fitted charges correlates
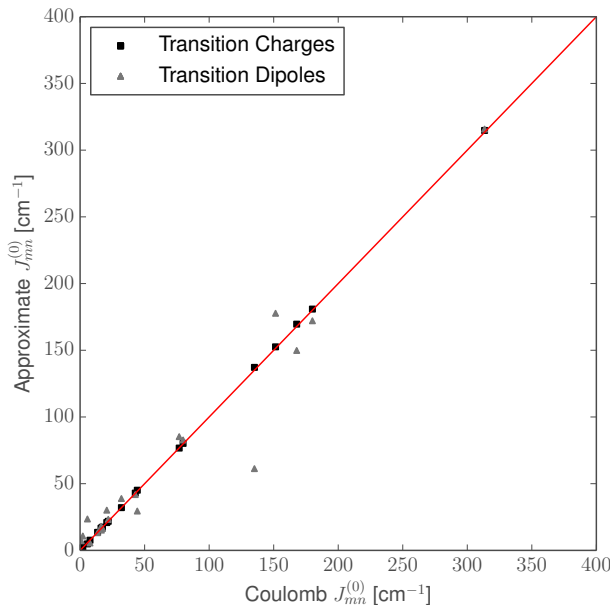
Figure 5: Correlation between exact Coulomb couplings and couplings obtained with either the point-dipole approximation (gray triangles) or charges fitted to reproduce the electrostatic potential of the transition density (black squares).

very nicely with the exact Coulomb couplings without significant outliners (discussed below). In the same figure, we observe that there are significant outliers when comparing the exact Coulomb couplings with couplings obtained by the point dipole approximation which can all be related to short separation distances (see Figure S3 in the supporting information for a plot of the couplings plotted as a function of the distance). For the shortest separations, the $J_{34}^{(0)}$, $J_{37}^{(0)}$ and $J_{56}^{(0)}$ couplings with center of mass distances of 12.1 Å, 11.8 Å and 11.2 Å, respectively, gives different results depending on which level of theory is applied. Here, the couplings evaluated using the transition dipole moments deviate from the exact Coulomb couplings by 74 cm^{-1}, 18 cm^{-1} and 27 cm^{-1}, respectively. At these distances, the point-dipole approximation breaks down as expected.[20] This breakdown is not observed for the couplings based on the transition density fitted charges which only deviate by 2 cm^{-1}, 1 cm^{-1} and 2 cm^{-1} from the exact Coulomb couplings, respectively. For the signed couplings (Tables S4 to S15 in the supporting information) we have chosen the following sign conven-

17

tion to deal with the arbitrariness of the sign of the transition moments stemming from the phase factor on the wave function: The sign is determined from the dot product of the transition dipole moment and positional vector between atoms C1 and C20 in the pigments (see Figure S2 in the supporting information). Furthermore, we have chosen the sign in such a way that the largest direct coupling, $J_{12}^{(0)}$, is always positive. Using this sign convention, the $J_{57}^{(0)}$ coupling is of particular interest because the exact Coulomb coupling and the couplings calculated using the transition density charges both pblackict the coupling to be -2 cm^{-1} but this coupling calculated using the transition dipole scheme pblackicts it to be $+11$ cm^{-1}. This particular case shows that the transition dipole moment approach cannot adequately describe the complexity of the transition density whereas the transition density fitted charge approach performs much better. The discrepancy between using either the transition density fitted charges or transition dipole moments is also observed when inspecting the mean signed error (MSE), the mean absolute error (MAE) and the root mean square error (RMSE) referenced to couplings obtained using the exact Coulomb expression. For the transition charges, these errors are -0.2 cm^{-1}, 0.5 cm^{-1} and 0.8 cm^{-1}, respectively. Using the corresponding transition dipole moment to evaluate the couplings gives MSE, MAE and RMSE values of 5.2 cm^{-1}, 10.3 cm^{-1} and 18.6 cm^{-1}, respectively.

Having observed that the EET couplings calculated based on transition density fitted charges are in excellent agreement with the exact Coulomb couplings, we now test the performance of the transition charge approach when blackucing the seven unique sets of charges into an average set of charges, $\{\bar{q}^T\}$. Using this average set of charges to evaluate the couplings, the mean signed error is -0.0 cm^{-1} which for all practical purposes is unchanged from the individual sets of charges. However, the mean absolute error increases to 4.7 cm^{-1} and the root mean square error increases to 7.7 cm^{-1}. This is perhaps not surprising because the local environment of each pigment is different from each other and the average charges cannot describe such complexity. From the average set of charges, it is possible to calculate an average transition dipole moment, $\bar{\boldsymbol{\mu}}^T$, for each pigment. Using this average

transition dipole we obtain errors of 6.1 cm^{-1}, 11.6 cm^{-1} and 18.6 cm^{-1} for MSE, MAE and RMSE, respectively. In conclusion we observe that the transition density charge model can very accurately reproduce the exact Coulomb couplings in all tested cases. Computing an average set of charges from the transition density charges yields appreciable accuracy, however, the heterogeneous environment lowers the accuracy of the obtained couplings. The transition dipole (and average transition dipole) moments both yield results which are of acceptable accuracy provided that there is some separation between the pigments. For close pairs of pigments this latter model causes significant errors in line with previous observations.[20] Overall, the computed $J_{mn}^{(0)}$ couplings using either the exact Coulomb expression or the transition density fitted charges is recommended for accuracy, but the latter is considerably cheaper than the former with only a very minor deviation in the computed couplings. Similarly to the direct couplings discussed above, the screenings, $J_{mn}^{(1)}$, again shows a large consistency when evaluated by either the exact transition density fields (eq 9) or the fields from the fitted charges (eq 12) which is exemplified in Figure 6 where the correlation between the total coupling (eq 5) and the exact Coulomb couplings are found to be very similar results for both approaches. To quantify the screening effect, we use an effective dielectric constant of the heterogeneous environment defined as[13,15,25]

$$\varepsilon_{\text{eff}} = \frac{J_{mn}^{(0)}}{J_{mn}^{(0)} + J_{mn}^{(1)}}. \tag{19}$$

From the slope of the correlation plots in Figure 6 we evaluate the average effective dielectric constant, $\langle \varepsilon_{\text{eff}} \rangle$, which we calculate to be 1.68 in excellent agreement with previous results for the FMO protein ($\langle \varepsilon_{\text{eff}} \rangle = 1.70$)[25]. The effect of the screening is to dampen the direct coupling due to the presence of the heterogeneous environment, through the electric dipole polarizabilites. The larger couplings are screened more heavily than the smaller ones, which is expected since the field strength, at the polarizable sites, just as the couplings, are directly dependent on the values of the transition charges (or transition density). The discrepancy is
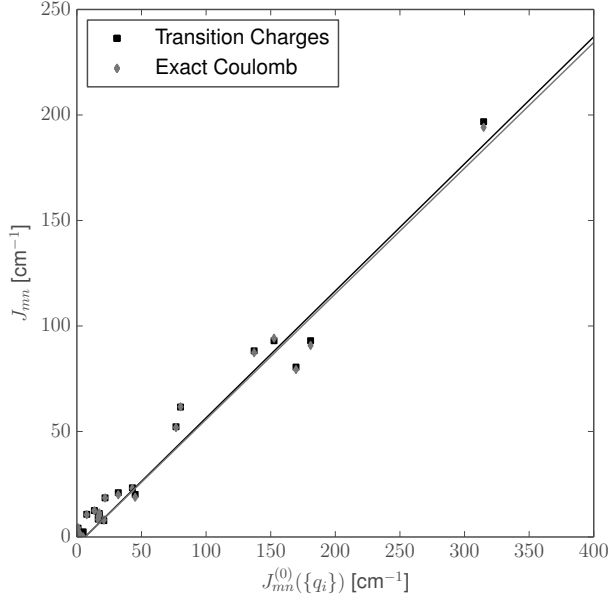
Figure 6: Total coupling, evaluated both exactly using a Coulomb expression and using partial charges fitted to reproduce the electrostatic potential of the transition density correlated with the direct coupling evaluated based on partial charges.

more noticeable when using transition dipole moments with MSE, MAE and RMSE values of 1.0 cm^{-1}, 7.1 cm^{-1}, 11.7 cm^{-1} when compablack to $J^{(1)}$ from the exact Coulomb expression. The effect of the screening between the pigments can be quite remarkable. For instance, the computed screening can, for small direct couplings, be larger in magnitude than the direct couplings ($J_{35}^{(1)}$ and $J_{37}^{(1)}$) leading to an total negative coupling. This is, in a perturbation description, not unreasonable and has been suggested before.[24] Furthermore, the screening can also enhance the coupling by having the same sign as the direct coupling. This is observed for $J_{25}^{(1)}$ which has a value of -3 cm^{-1} where the direct coupling is valued at -8 cm^{-1} obtained using a charge description. As was observed for the direct coupling, there is a sign difference of the $J_{57}^{(1)}$ screening dependent on whether it is evaluated with transition dipole moments or the transition density (or charges). However, the obtained signs of the screening is, despite this sign difference, consistent with the sign on the direct term and both effectively screens the total signed coupling except for the $J_{57}^{(1)}$ screening discussed above.

In light of the significant change in both excitation energies, the increase in transition

dipole moments and the magnitude of the computed couplings when including a polarizable environment described using an accurate embedding potential, we finish the discussion of the computed couplings by comparing (and contrasting) the obtained total couplings in this study (eq 5) with results from recent work in the literature. We have selected three recent studies which are based on the same initial structure of the FMO complex, but where the couplings have been calculated differently on both the theoretical and computational level. Table 1 lists our obtained total couplings calculated using the exact Coulomb expression for $J_{mn}^{(0)}$ (eq 10) and the corresponding $J_{mn}^{(1)}$ obtained at the PBE0/6-31+G* level of theory. This table also includes computed couplings evaluated through the exact Coulomb expression averaged over several snapshots extracted from a molecular dynamics simulation by Jurinovich et al.[25] We also include computed couplings obtained using the frozen density embedding[33–35] approach from König et al.[14] where we note that the computed couplings include some polarization in calculations through a series of "freeze and thaw" cycles. Finally, we include a study from Schmidt am Busch et al.[67] in which the couplings are evaluated using the point-dipole approximation with empirically scaled transition dipole moments. We observe that our computed couplings J_{mn} in general are comparable to both those obtained by Jurinovich et al. and König et al. with notable exceptions such as the J_{12}, J_{35} and J_{37} couplings which we will discuss in detail below. We note that the couplings obtained by Schmidt am Busch et al. are generally smaller than ours, which is to be expected, since the transition moments are empirically scaled to have a certain transition dipole moment length. The most startling difference from our results compablack to literature data is the magnitude of the J_{12} coupling which is increased by 33 cm^{-1} compablack to what is observed in ref 14, which also uses a geometry optimized structure. In our case, this coupling is comprised of a direct contribution $J_{12}^{(0)} = 313$ cm^{-1}, which we believe is quite large due to the inclusion of differential polarization based on our advanced polarizable force field which, as we have already discussed, yields a larger transition dipole moment. Furthermore, the screening of this coupling is $J_{12}^{(1)} = -119$ cm^{-1}, which is also quite large when compablack to the average

Table 1: Absolute values of calculated electronic couplings, J_{mn} in cm^{-1}. Note that the obtained J_{35} and J_{37} couplings are negative (see text for discussion).

n	m	This	Ref 25	Ref 14	Ref 67
1	2	194	137	161	95
1	3	12	6	8	6
1	4	8	8	8	6
1	5	10	9	8	7
1	6	19	27	32	15
1	7	8	5	8	12
2	3	62	47	48	30
2	4	11	10	16	8
2	5	11	7	0	2
2	6	20	11	24	13
2	7	10	6	8	6
3	4	87	60	73	59
3	5	-4	2	0	1
3	6	18	16	8	9
3	7	0	15	32	3
4	5	91	91	81	64
4	6	23	18	32	17
4	7	79	67	89	62
5	6	94	73	121	90
5	7	2	8	16	5
6	7	52	36	32	35

value from the Jurinovich et al. study where they obtained only $J_{12}^{(1)} \approx -3.5$ cm^{-1}. It has been suggested[24] that for small direct couplings, i.e. couplings below 10 cm^{-1}, the screening term $J_{mn}^{(1)}$ can enhance, rather than screen, the total coupling. Indeed this is what we observe for the J_{35} coupling. Here, the direct coupling is 1 cm^{-1} and the screening is -5 cm^{-1} yielding a negative total coupling.

4.3   Absorption Spectrum

Finally, we present and discuss in this section a simulated absorption spectrum of the FMO protein comprised of the seven BChla pigments. In Figure 7 we have shown the calculated coupled spectrum (solid blue) using the explicitly calculated total coupling, J_{mn}, calculated coupled (solid orange) spectrum using the effective dielectric constant determined above and the uncoupled (dashed blue) spectrum together with the experimental absorption spectrum recorded at 4K (solid black).[68] In this work, focus has been on the Q_y EET couplings and
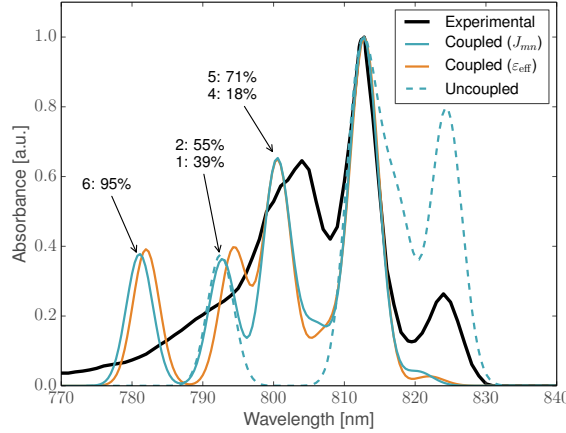

Figure 7: Simulated (blue and orange) absorption spectrum for the FMO protein calculated from uncoupled (dashed) and coupled (solid) transition moments from the exciton model. The experimental (4K) absorption spectrum obtained from ref 68 is shown in black. The simulated coupled and uncoupled absorption spectra were shifted 96 nm and 106 nm, respectively, to align the major peaks for easier comparison. Annotated peaks include only contributions larger than 10 %.

thus the simulated absorption spectra are shifted such that the major peaks are centered

on the major peak from the experimental spectrum for easier comparison. The computed spectra are broadened with Gaussian line shapes having a constant variance (σ) of 5 meV. We note that comparison to experiment is difficult in our case due to neglect of dynamical and vibrational effects.[25] However, here we focus on the effects of including / excluding the EET couplings in the computed spectrum and are thus less concerned with reproducing the experimental spectrum perfectly. We will discuss the obtained spectrum with special detail to the solid blue spectrum in Figure 7 evaluated from the total coupling but note that the spectrum obtained using the effective dielectric constant from the previous section (solid orange) is in overall agreement with the solud blue spectrum and will be a subject of future studies. Figure 7 is annotated with two outlying peaks centered around 781 nm and 793 nm and a peak that coincides with a peak on the experimental spectrum centered around 801 nm. The first peak of the coupled spectrum, centered around 781 nm, is comprised almost completely (95 %) of the Q_y excited state of pigment 6. As already discussed in the section on excitation energies and transition dipole moments, the location of this peak confirms that the environment surrounding pigment 6 is probably not representative for an experimental setup. Indeed, it has been reported previously that the site energies, contrary to the couplings, are very sensitive to both structural and environmental effects.[14] The other noticeable peak, centered around 793 nm, is comprised in almost equal parts of the Q_y excitation of pigment 1 and 2 and is a result of the strong coupling (≈ 200 cm^{-1}) between the two. The third peak, centered around 800 nm is mainly comprised of the Q_y excited states of pigments 5 and 4 which accounts for almost 90 % of that state. We note that the uncoupled spectrum does not have a peak around 800 nm. The major peak of the coupled spectrum is redshifted 10 nm compared the major peak in the uncoupled spectrum.

5 Summary and outlook

We have presented an analysis of three common computational approaches when evaluating electronic energy transfer couplings in an heterogeneous environment: Exact Coulomb, charges fitted to reproduce the electrostatic potential of the transition density and the point-dipole approximation based on transition dipoles. We used a perturbation expression for the total couplings which is comprised of a direct term and a screening term that takes into account the environmental response. We have used an advanced polarizable force field which has been derived from separate ab initio calculations which, compared to employing a standard protein force fields, takes into account structural effects in the embedding parameters. In terms of direct electronic couplings we conclude that using either the exact Coulomb approach or transition density fitted charges is preferable for accuracy but the latter is clearly preferable in terms of computational speed which is on par with the point-dipole approximation. In one case, the point-dipole approximation yields the wrong sign compared to the other two tested approaches emphasizing that this approach cannot always describe the complex nature of the transition density. We showed, in the perturbation formulation of the electronic couplings, that the screening may be written in terms of electric transition fields arising from either the transition density directly, fitted charges placed on the atoms of each pigment or transition dipole moments placed at the center of mass of the pigments. Again we found that the exact Coulomb approach and the fitted charges fitted yields very similar results while the point-dipole approximation shows some shortcomings. Even though the presented absorption spectrum for FMO is not representative of an experimental situation, the possibility to elucidate structural problems from a computed spectrum is of importance in for example the field of protein structure simulations where simulated structures are augmented with experimental data.[69] The use of the Frenkel exciton model allows for straight forward computation of other coupled optical properties such as circular dichroism. This will be explored in future studies.

Acknowledgement

Supporting Information Available

Figures S1 and S2 are graphical illustrations of Bachteriochlorophylls used in the fragmentation procedure to generate the classical potentials and as the quantum mechanical region in the embedded calculations, respectively. Table S1 contains center of mass and minimum inter-pigment distances. Tables S2 and S3 lists excited state energies and transition dipole moments for embedded pigments in both a static and polarizable environments. Tables S4 to S9 lists signed direct, screening and total electronic couplings for PBE0 and CAM-B3LYP. This material is available free of charge via the Internet at `http://pubs.acs.org/`.

Appendix

Electrostatic Potential Fitted Charges

A molecule with M nuclei and N electrons exhibits the following molecular electrostatic potential, $V^{\mathrm{ref}}(\mathbf{R}_a)$, at a point $\mathbf{R}_a$:

$$V^{\mathrm{ref}}(\mathbf{R}_a) = \sum_m^M \frac{Z_m}{|\mathbf{R}_m - \mathbf{R}_a|} - \sum_{\mu\nu} P_{\mu\nu} \int \mathrm{d}\mathbf{r}\chi_\mu(\mathbf{r})\frac{1}{|\mathbf{r} - \mathbf{R}_a|}\chi_\nu(\mathbf{r}), \qquad (20)$$

where Z_m is the nuclear charge of the m'th nuclei at position $\mathbf{R}_m$. The last term consists of the electron density in the atomic orbital (AO) basis, $P_{\mu\nu}$, multiplied by the one-electron potential integrals. We wish to find a set of M partial atomic charges, $\{q_m\}$ giving rise to an electrostatic potential at $\mathbf{R}_a$ according to

$$V^q(\mathbf{R}_a) = \sum_m^M \frac{q_m}{|\mathbf{R}_a - \mathbf{R}_m|}. \tag{21}$$

The charges are defined so as to minimize the difference between the electrostatic potential through eq 20 and the electrostatic potential produced by the M partial atomic charges through eq 21. The potential is evaluated in K points around the molecule. We use a Connolly surface[70] but in practice any surface can be used. To minimize the difference in electrostatic potentials, we use the following object function which is to be minimized

$$\gamma(\{q_m\}) = \sum_k^K (V^{\text{ref}}(\mathbf{R}_k) - V^q(\mathbf{R}_k))^2. \tag{22}$$

Constraints to restrict the sum of the partial charges to the total charge of the molecule, Q_{tot}, is included through a Lagrange multiplier

$$0 = g_1(\{q_m\}) = \sum_m^M q_m - Q_{\text{tot}}. \tag{23}$$

Likewise, the charges are constrained in such a way that the molecular dipole constructed from the partial charges must reproduce the permanent dipole moment of the molecule through three additional Lagrange multipliers: one for each Cartesian component of the dipole moment $\vec{\mu} = (\mu_x, \mu_y, \mu_z)$, i.e. for the μ_x-component

$$0 = g_2(\{q_m\}) = \sum_m^M q_m(x_m - R_{\text{cm},x}) - \mu_x. \tag{24}$$

Here, x_m is the x-coordinate of the m'th charge, q_m, and $\mathbf{R}_{cm}$ is the center of mass of the molecule under investigation. There are similar expressions for the y and z directions of the dipole moment. Combined, this gives the final object function to minimize

$$z(\{q_m\}) = \gamma(\{q_m\}) + \lambda_1 \cdot g_1(\{q_m\}) + \lambda_2 \cdot g_2(\{q_m\}) + \lambda_3 \cdot g_3(\{q_m\}) + \lambda_4 \cdot g_4(\{q_m\}). \quad (25)$$

To minimize this function, derivatives with respect to the charges $\{q_m\}$ and each of the constraints λ_i are taken. This gives rise to a set of linear equations which can be solved by traditional linear algebra manipulations[71,72]. To avoid numerical problems we use the singular value decomposition approach. In this work, the EET couplings are determined from transition densities. By evaluating eq 20 using a transition density, one obtains *transition density fitted charges* provided that the nuclear charges are set to zero, the overall charge is set to zero (no charge is generated or removed, only moved around) and that the dipole moment is constrained to reproduce the transition dipole moment of the excitation. This procedure is similar to that of TrESP[22]. The above has been implemented in a separate charge fitting module called QFIT[64] in the DALTON[61] program package.

References

(1) Scholes, G. D. *Annu. Rev. Phys. Chem.* **2003**, *54*, 57–87.

(2) Cheng, Y.-C.; Fleming, G. R. *Annu. Rev. Phys. Chem.* **2009**, *60*, 241–262.

(3) Frenkel, J. *Phys. Rev.* **1931**, *37*, 17–44.

(4) Renger, T.; May, V.; Kühn, O. *Phys. Rep.* **2001**, *343*, 137–254.

(5) Renger, T.; Müh, F. *Phys. Chem. Chem. Phys.* **2013**, *15*, 3348.

(6) Cole, D. J.; Chin, A. W.; Hine, N. D. M.; Haynes, P. D.; Payne, M. C. *J. Phys. Chem. Lett.* **2013**, *4*, 4206–4212.

(7) Warshel, A.; Parson, W. W. *J. Am. Chem. Soc.* **1987**, *109*, 6143–6152.

(8) Damjanović, A.; Ritz, T.; Schulten, K. *Phys. Rev. E.* **1999**, *59*, 3293–3311.

(9) Beljonne, D.; Cornil, J.; Silbey, R.; Millié, P.; Brédas, J. L. *J. Chem. Phys.* **2000**, *112*, 4749.

(10) Müh, F.; Madjet, M. E.-A.; Adolphs, J.; Abdurahman, A.; Rabenstein, B.; Ishikita, H.; Knapp, E.-W.; Renger, T. *PNAS* **2007**, *104*, 16862–16867.

(11) Adolphs, J.; Müh, F.; Madjet, M. E.-A.; Renger, T. *Photosynth Res* **2007**, *95*, 197–209.

(12) Chen, H.-C.; You, Z.-Q.; Hsu, C.-P. *J. Chem. Phys.* **2008**, *129*, 084708.

(13) Curutchet, C.; Kongsted, J.; Muñoz-Losa, A.; Hossein-Nejad, H.; Scholes, G. D.; Mennucci, B. *J. Am. Chem. Soc.* **2011**, *133*, 3078–3084.

(14) König, C.; Neugebauer, J. *J. Chem. Theory Comput.* **2013**, *9*, 1808–1820.

(15) Jurinovich, S.; Viani, L.; Curutchet, C.; Mennucci, B. *Phys. Chem. Chem. Phys.* **2015**,

(16) Olsen, J. M.; Aidas, K.; Kongsted, J. *J. Chem. Theory Comput.* **2010**, *6*, 3721–3734.

(17) Olsen, J. M. H.; Kongsted, J. *Advances in Quantum Chemistry*; Elsevier BV, 2011; pp 107–143.

(18) Förster, T. *Ann. Phys.* **1948**, *437*, 55–75.

(19) Renger, T. *Photosynth. Res.* **2009**, *102*, 471–485.

(20) Muñoz-Losa, A.; Curutchet, C.; Krueger, B. P.; Hartsell, L. R.; Mennucci, B. *Biophys. J.* **2009**, *96*, 4779–4788.

(21) Krueger, B. P.; Scholes, G. D.; Fleming, G. R. *J. Phys. Chem. B* **1998**, *102*, 5378–5386.

(22) Madjet, M. E.; Abdurahman, A.; Renger, T. *J. Phys. Chem. B* **2006**, *110*, 17268–17281.

29

(23) Fujimoto, K. J. *J. Chem. Phys.* **2014**, *141*, 214105.

(24) Hsu, C.-P.; Fleming, G. R.; Head-Gordon, M.; Head-Gordon, T. *J. Chem. Phys.* **2001**, *114*, 3065.

(25) Jurinovich, S.; Curutchet, C.; Mennucci, B. *ChemPhysChem* **2014**, *15*, 3194–3204.

(26) Knox, R. S.; Spring, B. Q. *Photochem. Photobiol.* **2003**, *77*, 497–501.

(27) Iozzi, M. F.; Mennucci, B.; Tomasi, J.; Cammi, R. *J. Chem. Phys.* **2004**, *120*, 7029.

(28) Curutchet, C.; Mennucci, B. *J. Am. Chem. Soc.* **2005**, *127*, 16733–16744.

(29) Curutchet, C.; Scholes, G. D.; Mennucci, B.; Cammi, R. *J. Phys. Chem. B* **2007**, *111*, 13253–13265.

(30) Curutchet, C.; Muñoz-Losa, A.; Monti, S.; Kongsted, J.; Scholes, G. D.; Mennucci, B. *J. Chem. Theory Comput.* **2009**, *5*, 1838–1848.

(31) Steinmann, C.; Olsen, J. M. H.; Kongsted, J. *J. Chem. Theory Comput.* **2014**, *10*, 981–988.

(32) Olsen, J. M. H.; Steinmann, C.; Ruud, K.; Kongsted, J. *J. Phys. Chem. A* **2015**, 150202123644004.

(33) Wesolowski, T. A.; Warshel, A. *J. Phys. Chem.* **1993**, *97*, 8050–8053.

(34) Casida, M. E.; Wesołowski, T. A. *Int. J. Quantum Chem.* **2004**, *96*, 577–588.

(35) Neugebauer, J. *J. Chem. Phys.* **2007**, *126*, 134116.

(36) Neugebauer, J. *ChemPhysChem* **2009**, *10*, 3148–3173.

(37) Mennucci, B.; Curutchet, C. *Phys. Chem. Chem. Phys.* **2011**, *13*, 11538.

(38) Fenna, R. E.; Matthews, B. W. *Nature* **1975**, *258*, 573–577.

(39) Matthews, B.; Fenna, R.; Bolognesi, M.; Schmid, M.; Olson, J. *J. Mol. Biol.* **1979**, *131*, 259–285.

(40) Tronrud, D. E.; Wen, J.; Gay, L.; Blankenship, R. E. *Photosynth. Res.* **2009**, *100*, 79–87.

(41) Wen, J.; Zhang, H.; Gross, M. L.; Blankenship, R. E. *Biochemistry* **2011**, *50*, 3502–3511.

(42) Patwardhan, S.; Tonzani, S.; Lewis, F. D.; Siebbeles, L. D. A.; Schatz, G. C.; Grozema, F. C. *J. Phys. Chem. B* **2012**, *116*, 11447–11458.

(43) Nielsen, L. M.; Hoffmann, S. V.; Nielsen, S. B. *Photochem. Photobiol. Sci.* **2013**, *12*, 1273.

(44) List, N. H.; Curutchet, C.; Knecht, S.; Mennucci, B.; Kongsted, J. *J. Chem. Theory Comput.* **2013**, *9*, 4928–4938.

(45) Maestro, version 10.0, Schrödinger, Inc., New York, NY, 2014.

(46) Söderhjelm, P.; Ryde, U. *J. Phys. Chem. A* **2009**, *113*, 617–627.

(47) Zhang, D. W.; Zhang, J. Z. H. *J. Chem. Phys.* **2003**, *119*, 3599.

(48) Olsen;, J. M. H. Development of Quantum Chemical Methods towards Rationalization and Optimal Design of Photoactive Proteins. 2013; `http://dx.doi.org/10.6084/m9.figshare.156852`, (accessed June 20th, 2015).

(49) Becke, A. D. *J. Chem. Phys.* **1993**, *98*, 5648–5652.

(50) Vosko, S. H.; Wilk, L.; Nusair, M. *Can. J. Phys.* **1980**, *58*, 1200–1211.

(51) Lee, C.; Yang, W.; Parr, R. G. *Phys. Rev. B* **1988**, *37*, 785–789.

(52) Hehre, W. J.; Ditchfield, R.; Pople, J. A. *J. Chem. Phys.* **1972**, *56*, 2257– 2261.

(53) Hariharan, P. C.; Pople, J. A. *Theor. Chim. Acta* **1973**, *28*, 213–222.

(54) Clark, T.; Chandrasekhar, J.; Spitznagel, G. W.; Schleyer, P. V. R. *J. Comput. Chem.* **1983**, *4*, 294–301.

(55) Gagliardi, L.; Lindh, R.; Karlström, G. *J. Chem. Phys.* **2004**, *121*, 4494–4500.

(56) Karlström, G.; Lindh, R.; Malmqvist, P.-Å.; Roos, B. O.; Ryde, U.; Veryazov, V.; Widmark, P.-O.; Cossi, M.; Schimmelpfennig, B.; Neogrady, P.; Seijo, L. *Comput. Mater. Sci.* **2003**, *28*, 222–239.

(57) Aquilante, F.; De Vico, L.; Ferré, N.; Ghigo, G.; Malmqvist, P.-Å.; Neogrády, P.; Pedersen, T. B.; Pitoňák, M.; Reiher, M.; Roos, B. O.; Serrano-Andrés, L.; Urban, M.; Veryazov, V.; Lindh, R. *J. Comput. Chem.* **2010**, *31*, 224–247.

(58) Steinmann, C.; Ibsen, M. W.; Hansen, A. S.; Jensen, J. H. *PLoS ONE* **2012**, *7*, e44480.

(59) Adamo, C.; Barone, V. *J. Chem. Phys.* **1999**, *110*, 6158.

(60) Yanai, T.; Tew, D. P.; Handy, N. C. *Chem. Phys. Lett.* **2004**, *393*, 51–57.

(61) Aidas, K.; Angeli, C.; Bak, K. L.; Bakken, V.; Bast, R.; Boman, L.; Christiansen, O.; Cimiraglia, R.; Coriani, S.; Dahle, P.; Dalskov, E. K.; Ekström, U.; Enevoldsen, T.; Eriksen, J. J.; Ettenhuber, P.; Fernández, B.; Ferrighi, L.; Fliegl, H.; Frediani, L.; Hald, K.; Halkier, A.; Hättig, C.; Heiberg, H.; Helgaker, T.; Hennum, A. C.; Hettema, H.; Hjertenaes, E.; Høst, S.; Høyvik, I.-M.; Iozzi, M. F.; Jansík, B.; Jensen, H. J. A.; Jonsson, D.; Jørgensen, P.; Kauczor, J.; Kirpekar, S.; Kjaergaard, T.; Klopper, W.; Knecht, S.; Kobayashi, R.; Koch, H.; Kongsted, J.; Krapp, A.; Kristensen, K.; Ligabue, A.; Lutnaes, O. B.; Melo, J. I.; Mikkelsen, K. V.; Myhre, R. H.; Neiss, C.; Nielsen, C. B.; Norman, P.; Olsen, J.; Olsen, J. M. H.; Osted, A.; Packer, M. J.; Pawlowski, F.; Pedersen, T. B.; Provasi, P. F.; Reine, S.; Rinkevicius, Z.; Ruden, T. A.; Ruud, K.; Rybkin, V. V.; Sałek, P.; Samson, C. C. M.; de Merás, A. S.; Saue, T.;

Sauer, S. P. A.; Schimmelpfennig, B.; Sneskov, K.; Steindal, A. H.; Sylvester-Hvid, K. O.; Taylor, P. R.; Teale, A. M.; Tellgren, E. I.; Tew, D. P.; Thorvaldsen, A. J.; Thøgersen, L.; Vahtras, O.; Watson, M. A.; Wilson, D. J. D.; Ziolkowski, M.; Ågren, H. *WIREs Comput Mol Sci* **2013**, *4*, 269–284.

(62) Dalton, a Molecular Electronic Structure Program, Release Dalton2015.0 (2015), see http://daltonprogram.org/ (accessed June 22, 2015).

(63) Olsen, J. M. H. PElib: The Polarizable Embedding library (version 1.0.8). 2014.

(64) Steinmann, C. qfitlib-1.0.4. 2015; `http://dx.doi.org/10.5281/zenodo.14949`, (accessed June 22nd, 2015).

(65) Kaminski, G. A.; Friesner, R. A.; Tirado-Rives, J.; Jorgensen, W. L. *J. Phys. Chem. B* **2001**, *105*, 6474–6487.

(66) Adolphs, J.; Renger, T. *Biophys. J.* **2006**, *91*, 2778–2797.

(67) Schmidt am Busch, M.; Müh, F.; Madjet, M. E.-A.; Renger, T. *J. Phys. Chem. Lett.* **2011**, *2*, 93–98.

(68) Wendling, M.; Przyjalgowski, M. A.; Gülen, D.; Vulto, S. I. E.; Aartsma, T. J.; van Grondelle, R.; van Amerongen, H. *Photosynth. Res.* **2002**, *71*, 99–123.

(69) Shaw, D. E.; Maragakis, P.; Lindorff-Larsen, K.; Piana, S.; Dror, R. O.; Eastwood, M. P.; Bank, J. A.; Jumper, J. M.; Salmon, J. K.; Shan, Y.; Wriggers, W. *Science* **2010**, *330*, 341–346.

(70) Connolly, M. L. *J. Appl. Crystallogr.* **1983**, *16*, 548–558.

(71) Hinsen, K.; Roux, B. *J. Comput. Chem.* **1997**, *18*, 368–380.

(72) Sigfridsson, E.; Ryde, U. *J. Comput. Chem.* **1998**, *19*, 377–395.

Graphical TOC Entry

$J = J^{(0)} + J^{(1)}$